Published in final edited form as:
Langmuir. 2012 October 9; 28(40): 14415–14423. doi:10.1021/la302428a.

Irradiation Induced Fluorescence Enhancement in PEGylated Cyanine-based NIR Nano- and Meso-scale GUMBOS

Chengfei Lu, **Susmita Das**, **Paul K. S. Magut**, **Min Li**, **Bilal El Zahab**, and **Isiah M. Warner***
Department of Chemistry, Louisiana State University, Baton Rouge, LA70803, USA

Abstract

We report on the synthesis and characterization of a PEGylated IR786 GUMBOS (Group of Uniform Materials Based on Organic Salts). The synthesis of this material was accomplished using a three step protocol: (1) substitution of chloride on the cyclohexenyl ring in the heptamethine chain of IR786 by 6-aminohexanoic acid, (2) grafting of methoxy poly ethyleneglycol (MeOPEG) onto the 6-aminohexanoic acid via an esterification reaction, and (3) anion exchange between [PEG786][I] and lithium bis(trifluoromethylsulfonyl)imide ($LiNTf_2$) or sodium bis(2-ethylhexyl)sulfosuccinate (AOT) in order to obtain PEG786 GUMBOS. Examination of spectroscopic data for this PEG786 GUMBOS indicates a large stokes shift (122 nm). It was observed that this PEG786 GUMBOS associates in aqueous solution to form nano-and meso-scale self-assemblies with sizes ranging from 100 to 220 nm. These nano- and meso-scale GUMBOS are also able to resist nonspecific binding to proteins. PEGylation of the original IR786 leads to reduced cytotoxicity. In addition, it was noted that anions, such as NTf_2 and AOT, play a significant role in improving the photostability of PEG786 GUMBOS. Irradiation-induced J aggregation in [PEG786][NTf_2] and to some extent in [PEG786][AOT] produced enhanced photostability. This observation was supported by use of both steady state and time-resolved fluorescence measurements.

Keywords

NIR dye; PEGylation; Fluorescence Enhancement; GUMBOS

1. Introduction

Fluorescent nanoparticles have been widely studied as diagnostic and thermal therapeutic agents with applications to tumor imaging and targeted cancer drug delivery. [1-7] Nanoparticles that can absorb and emit light in the near-infrared (NIR) region are of great interest in biomedical applications since the skin has minimum absorption coefficient and maximum penetration depth for electromagnetic radiation in the NIR region.[8, 9] There are numerous fluorescent NIR materials or molecules available which can be employed to

* Corresponding author, Isiah M. Warner iwarner@lsu.edu, Phone: 1-225-578-2829.

Supporting Information Available:
NMR characterization and EMI-MS analysis of the intermediate product and the synthesized GUMBOS, transformation of pyramidal geometry to planar configuration, UV-vis absorption spectra of [IR786][I] and [PEG786][I] and different spectra for [IR786][I] and [PEG786][I] binding to BSA are also provided. This material is available free of charge via the Internet at http://pubs.acs.org.

provide fluorescence property in nanoparticles. These include quantum dots,[10, 11] fluorescent protein,[12, 13] gold/silver nanoparticles[14], and fluorescent NIR organic molecules.[8, 15-17] Among these, NIR organic dyes have become the most frequently used fluorophores in fluorescent probes for imaging vascular pathophysiology and other disorders.[9, 18] This is due to their low toxicity, low cost, and easy conjugation with functional groups.[19] Two methods have been developed to prepare fluorescent NIR organic nanoparticles. One involves encapsulation of organic molecules in nanocomposite particles;[9] the other uses a reprecipitation method to prepare nanoparticles employing water-insoluble dyes.[20, 21]

Among various organic fluorescent NIR dyes, heptamethine cyanine dyes are promising candidates due to their high molar extinction coefficients and broad wavelength tunability.[22, 23] However, when used as optical contrast agents, the heptamethine cyanine dyes suffer from several disadvantages. These major disadvantages which limit the application of cyanine dyes for biomedical applications include low quantum yields, self-assembly to form non-fluorescent aggregates, short fluorescence lifetime, poor photostability, cytotoxicity, non-specific binding to proteins and other cell components[24], and small Stokes shifts.[25] To improve the properties of heptamethine cyanine dyes, much effort has been directed toward modification of the molecular structures of these dyes. For example, studies have demonstrated that cyanine dyes which incorporate a rigid cyclohexenyl ring in the heptamethine chain have increased photostability and enhanced quantum yield as compared to cyanine dyes with an open polymethine chain.[26] In addition, cyanine dyes with two sulfonic groups or carboxyl groups have improved photostability, increased water solubility, as well as greater biocompatibility. For example, indocyanine green (ICG), a cyanine dye with two sulfonic groups, has been approved by the U.S Food and Drug Administration (FDA) for human use due to its low toxicity (LD_{50} of 50-80 mg/kg for animal subjects).[9]

For most heptamethine cyanine dyes, Stokes shifts are often less than 25 nm, which can result in self-quenching and measurement errors from excitation and scattered light.[25] Peng, et al. have reported new cyanine dyes which have large Stokes shifts (>140 nm)[27]. These new dyes are derived from cyanine dyes containing a central cyclohexenyl ring in the heptamethine chain. A robust C-N bond substitution at the C-Cl bond on the rigid ring leads to a large Stoke shift due to excited-state intramolecular charge transfer (ICT) between a donor and acceptor in the dyes. However, most of these modifications were employed using cyanine dyes which are water soluble. Water soluble dyes cannot self-assemble to produce nanoparticles in aqueous solution using a reprecipitation method. In contrast, the research reported in this manuscript focuses on modification of water insoluble heptamethine cyanine dyes to produce stable self-assemblies in aqueous solution by use of reprecipitation.

PEG is a water soluble and biocompatible polymer that has been widely used to modify the surface properties of various nanoparticles.[28-31] The surface properties of nanoparticles, e.g. hydrophobicity, play an important role in stabilizing such nanoparticles, which in turn determines the *in vivo* fate of these nanoparticles. It is well established that nanoparticles with hydrophobic surfaces are rapidly captured and massively cleared by the mononuclear phagocyte system (MPS). Upon PEGylation, the hydrophilicity of the PEG chain will

typically prevent such nanoparticles from being recognized by MPS.[32] Moreover, PEG chains extend into the aqueous pool and provide a sphere of solvation in water , thus preventing such dyes from aggregating.[33] In addition, a PEG shell has the potential of reducing non-specific binding to proteins[34] , as well as reducing cytotoxicity. [35]

Our group has recently reported a series of organic salts which are similar to ionic liquids, but do not fit the accepted definition of ionic liquids since they often have melting points greater than 100 ° C.[20, 21] We have defined these materials as a **g**roup of **u**niform **m**aterials **b**ased on **o**rganic **s**alts and use the acronym, GUMBOS, to describe these materials with melting points between 25 °C and 250 °C. As used here, GUMBOS can be singular and plural.

Cyanine dyes are typically either cationic or anionic organic salts. Dyes with two sulfonic groups or carboxyl groups are anionic salts with typically small counter cations, such as sodium. Dyes without negatively charged groups are cationic salts with counter anions, such as iodide ion. Since various anions are available for conversion to GUMBOS, cationic cyanine dye based GUMBOS can be obtained by use of anion-exchange. It has been demonstrated that cationic cyanine dyes coupled with various anions display tunable spectral properties in aqueous solutions.[21] Therefore, in this article, selection of a water insoluble cyanine dye (cationic) for modification is based on considerations of exploiting these anion controlled spectral properties.

In this study, in order to achieve large stokes shift, lower non-specific binding to proteins, and to reduce cytotoxicity, 6-aminohexanoic acid linked with PEG was used to modify IR786, which is normally a water insoluble cationic NIR dye with a rigid cyclohexenyl ring in the heptamethine chain. The modified dye based GUMBOS were obtained by use of anion exchange with sulfosuccinate (AOT) sodium salt and lithium bis(trifluoromethane) sulfonamide (NTf_2), respectively. In this manuscript, we demonstrate that PEGylated dye-based GUMBOS show increased Stokes shifts and can form nano- and meso-sized self-assemblies in aqueous solution. The nano- and meso-scale GUMBOS also displayed anion and concentration dependent photostability as a result of irradiation. The PEG chains provide a protective outer layer for improving steric stabilization and reducing non-specific binding to protein and cytotoxicity.

2. Experimental Methods

2.a Materials

IR786 iodide, 6-aminohexanoic acid, DMF, polyethylene glycol monomethyl ether (MeOPEG, Mn=550), 1, 3 dicyclohexylcarbodiimide (DCC), bis(2-ethylhexyl) sulfosuccinate (AOT) sodium salt (≥99%), and lithium bis(trifluoromethane) sulfonamide (NTf_2) were all purchased from Sigma Aldrich and used as received. Four (4)-(Dimethylamino)pyridine (DMAP) and triethylamine were obtained from Fluka and Fisher Scientific respectively. Triply deionized water (18.2MΩ cm), obtained from an Elga model PURELAB ultra water-filtration system, and was used for the preparation of all PEGylated NIR dye samples.

2.b. Synthesis of PEG786 GUMBOS

The PEGylated NIR GUMBOS were synthesized by use of a two-step procedure followed by an anion exchange reaction. In the two-step reaction, 6-aminohexanoic acid was first attached to IR786 iodide ([IR786][I]) using a method described in the literature[23]. In this procedure, triethylamine (198 μL, 1.42 mmol) and 6-aminohexanoic acid (126 mg, 1.42 mmol) were added to a solution of IR786 iodide (0.283 mmol) in anhydrous DMF (10 mL) under nitrogen atmosphere. After stirring for 3 h at 85°C, the green solution changed to a blue solution. Flash chromatography (AcOEt/MeOH 70/30 to 0/100) was used to obtain a pure blue product (85% yield). Subsequently, 0.03 g of MeOPEG (0.06 mmol) and 0.02g of N, N- dimethylaminopyridine (DMAP) were dissolved in 10 mL of anhydrous DMSO. In a separate vessel, 0.0466 g of the blue compound (0.06 mmol) was dissolved into 10 mL of anhydrous DMSO together with 0.0124 g N, N -dicyclo-hexylcarbodiimide (DCC, 0.06 mmol). The mixture was stirred for 30 min at room temperature and then added to the above MeOPEG solution. This reaction mixture was then agitated for 2 days at room temperature (75% yield).

An anion exchange method similar to those reported in the literature was employed to prepare PEG786 GUMBOS.[21] Equimolar amounts of PEG786 iodide([PEG786][I]) and sodium bis(2-ethylhexyl) sulfosuccinate (AOT) salt were dissolved in a mixture of methylene chloride and water (2:1 v/v) and stirred for 12 h at room temperature. The methylene chloride bottom layer was washed several times with fresh water to remove the byproduct, NaI. The product ([PEG786][AOT], 80% yield) was obtained from the lower organic layer and dried after solvent removal under vacuum. A similar anion-exchange procedure was employed for preparation of [PEG786][NTf_2]. Detailed information about characterization of the products by use of NMR and ESI MS is provided in supporting information.

2.c. Preparation and Characterization of PEG786 nano- and meso-scale GUMBOS

The PEG786 nano- and meso-scale GUMBOS were prepared from PEG786 GUMBOS by use of a reprecipitation method which has been previously described in the literature. [20, 21] A given amount (1-70μL) of a 1 mM GUMBOS ethanolic solution of the GUMBOS was rapidly injected into 1 mL of triply deionized water in an ultrasonic bath (100 W), followed by additional sonication for 5 min.

The average particle sizes and morphologies of the prepared PEG786 nano- and meso-scale GUMBOS were obtained using transmission electron microscopy (TEM). These TEM micrographs were recorded by use of an LVEM5 transmission electron microscope (DelongAmerica, Montreal, Canada). A small amount of PEG786 nano- andmeso-scale GUMBOS in aqueous solution was drop cast onto a carbon-coated copper grid and allowed to dry in air at room temperature before TEM imaging. Electron diffraction measurements of the dried nano- and meso-scale GUMBOS were obtained on a Nonius Kappa CCD diffractometer through long exposure to Mo KR radiation and rotation of samples about the vertical axis.

2. d. Absorption and Fluorescence studies of PEG786 nano- and meso-scale GUMBOS

For all spectroscopic measurements, samples were placed in a low-volume fluorescence cuvet and held in place by use of a modified cuvet holder. UV-Vis-NIR absorption spectra were recorded using a UV-3101PC UV-Vis-NIR scanning spectrophotometer (Shimadzu). UV-Vis-NIR absorbance was performed and monitored in the wavelength range from 200 nm to 900 nm. Fluorescence spectra were recorded at room temperature by use of a Spex Fluorolog-3 spectrofluorimeter (model FL3-22TAU3; Jobin Yvon, Edison, NJ, USA) equipped with a 450-W xenon lamp and R928P photomultiplier tube (PMT) emission detector. The photostabilities of these PEG-modified dyes were evaluated in aqueous solution by excitation at 630 nm for 3000 seconds with 14nm slit width.

Fluorescence lifetime measurements were performed on a Spex Fluorolog-3 spectrofluorimeter (model FL3-22TAU3, Jobin Yvon, Edison, NJ) using time domain mode. A picosecond pulsed excitation source of 735 nm was used and emission collected at 760 nm with a TBX detector. The time correlated single photon counting (TSCPC) mode was used for data acquisition with a resolution of 7 ps/channel.

2.e. Study of Resistance to Non-specific Protein Adsorption

Absorption difference spectroscopy was used to study the resistance of PEG786 nano- and meso-scale GUMBOS to protein adsorption. Differential spectral titrations were performed at room temperature. [36] The concentration of the dye in the reference cuvet and the dye in the dye/BSA mixture were identical. The conditions employed were as follows:

1. At a constant dye concentration of 20 μM in PBS solutions (pH = 7.4), the BSA concentration was varied as follows: 0.1mg/mL, 0.2 mg/mL, 0.3 mg/mL, 0.4 mg/mL, 0.5 mg/mL, and 0.6 mg/mL;
2. At a constant concentration of 0.5 mg/mL BSA in PBS solutions (pH=7.4), the dye concentration was increased from 5μM to 20 μM;
3. The dye and BSA mixtures were then incubated for 1 hour before UV-vis-NIR absorption measurements.

2.f. In vitro Cytotoxicity Assay

Cytotoxicities of IR786 and PEG786 GUMBOS against HeLa cancer cell line were determined by use of an MTT Assay kit (Promega Corporation, Madison, WI, USA) according to the manufacturer's instructions. Briefly, in a 96-well plate, ~5000 cells in 0.1 mL culture medium were seeded to each well. After 24 h, the old culture medium was removed and discarded and 0.1 mL of new culture medium containing 0-40 μM [IR786][I] or PEG786 GUMBOS dissolved in 1% DMSO was introduced to the cells. The cells were then incubated for 48 h at 37 °C and 5% CO_2, in a humidified incubator. At the end of the incubation period, the cells were treated with 15 μL 3-(4, 5-Dimethylthiazol-2-yl)-2, 5-diphenyltetrazolium bromide (MTT) and incubated for 2 h. After two hours, 100 μL of the stop solution were added per well and incubated overnight. Cell viability was determined by reading the absorbance at 570 nm with a reference wavelength of 650 nm using a micro plate spectrophotometer (Benchmark Plus, Bio-Rad Laboratories, Hercules, CA, USA).

3. Results and discussion

The position of the chloride on the central cyclohexenyl ring of [IR786][I] is considered to be a useful reaction site for further structural modification. Six (6)-aminohexanoic acid, which has two functional groups, was linked to [IR786][I] by use of an $S_{NR}1$ reaction (Scheme 1, first reaction). Afterwards, polyethylene glycol monomethyl ether (MeoPEG) was attached to 6-aminohexanoic acid by use of an esterification reaction between the carboxyl and hydroxyl groups (Scheme 1, second reaction). Finally, the PEG786 GUMBOS were synthesized employing an anion exchange between [PEG786][I] and bis(2-ethylhexyl) sulfosuccinate (AOT) sodium salt (≥99%), lithium bis(trifluoromethane) sulfonamide (NTf_2) (Scheme 1, third reaction).

PEG786 GUMBOS formed nano sized self-assemblies in aqueous solution when a reprecipitation method was employed.[19,20] These nano- and meso-scale GUMBOS were characterized using transmission electron microscopy (TEM) (Figure 1). The TEM images of [PEG786][NTf_2] show that these nano- and meso-scale GUMBOS were primarily spherical with average diameters in the range of 100 to 220 nm; while [PEG786][I] nano- and meso-scale GUMBOS displayed both spherical and quasi spherical particles with average size ranging from 100 to 150 nm.

3.a. Spectroscopic Analysis of PEG786 GUMBOS

The PEG786 GUMBOS exhibited broader spectra as compared to the original unmodified IR786 (Figure 2). The absorption maxima of [PEG786][I] was observed at 620 nm which was 150 nm blue shifted as compared to its non-PEGylated counterpart. A large Stokes shift of 122 nm was also observed as compared to IR786 with a Stokes shift of 25 nm. The significant increase in Stokes shift after substitution of C-Cl bond with a C-N bond on the central ring is attributed to intramolecular charge transfer (ICT).[27] After structural modification, the nitrogen binding to the cyclohexenyl ring results in a bridgehead amine, which leads to intramolecular charge transfer (ICT). Accompanying ICT, a locally excited (LE) state (pyramidal geometry) is formed after excitation, and then transformed into an ICT state (planar configuration).[26] This process is illustrated in Scheme S1 of the supporting information.

3.b. Photostability of PEG786 Nano- and meso-scale GUMBOS

The stability of dyes, including the ability to resist degradation from light, heat, oxygen, and ozone, is important for spectroscopic applications.[37] For example, as optical contrast agents, cyanine dyes should have high photostability in order to improve their lifetimes for laser operation. In order to track the photobleaching of PEG786 GUMBOS, aqueous solutions of this compound were irradiated by use of a xenon lamp (630nm, slits 14/14) over a period of 50 min to examine irradiation photostability. A decrease in the emission maxima over time was recorded and is illustrated in Figures 3. As seen in Figure 3A, at a concentration of 20 μM, the photostability of [PEG786][AOT] was much higher than that of [PEG786][NTf_2] and [PEG786][I]. [PEG786][I] has the lowest photostability with a residual emission intensity of 15%. The residual emission intensity for [PEG786][AOT] and [PEG786][NTf_2] are 57% and 35%, respectively.

The effect of concentration on photostability of PEG786 GUMBOS in aqueous solution was also investigated. The results shown in Figure 3B, C and D indicate that photostability of three PEG786 nano- and meso-scale GUMBOS from 20 μM to 70 μM in water. It was observed that for [PEG786][I] the photostability dropped at all concentrations over a period of 50 min. However, for [PEG786][NTF_2] nano- and meso-scale GUMBOS, the higher concentrations exhibited an increase in fluorescence intensity after irradiating for more than 500 sec. Similar behavior was observed for [PEG786][AOT] at higher concentrations.

The emission spectrum of [PEG786][NTf_2] has a maximum at 742 nm and a shoulder at 798 nm (Figure 4A). Interestingly, it was observed that the photostability of [PEG786][NTF_2] increased upon short irradiation at all concentrations when the emission was collected at the shoulder (798 nm). Data from Figure 4B demonstrates that the ratio of residual emission intensity to emission intensity before irradiation at 798 nm was much higher than that at 742 nm: ratios of 65%, 160% and 160% at 798 nm were obtained as compared to 35%, 53% and 90% at 742nm with respective concentrations of 20 μM, 50 μM and 70 μM. The sharp increase in emission intensity at 798 nm after irradiation as compared to that before irradiation suggests that a new emitting species is formed due to irradiation which emits near 798 nm and has a higher quantum yield as compared to the initial emitting species.

Emission and excitation spectra of PEG786 nano- and meso-scale GUMBOS were obtained before and after irradiation. As a comparison, emission and excitation spectra without irradiation were also investigated to identify the new emitting species and understand the mechanism of formation. Figure 5A shows the excitation and emission spectra of [PEG786][NTf_2] (50 μM) before and after irradiation. Both the excitation and emission maxima exhibited a red shift after 50 min of irradiation. The excitation maximum shifted from 625 nm to 640 nm and the emission maximum shifted from 640 nm to 773 nm. These new maxima were ascribed to the new emitting species, which needs identification. Time studies of [PEG786][NTf_2] aqueous solution without irradiation were performed by recording the excitation and emission spectra at 15 min interval. The final spectrum was recorded at 50 minutes. The results are shown in Figure 5B and C. No peak shift was observed during time studies, which indicates that formation of the new emitting species is induced by irradiation rather than time. Moreover, such a phenomenon was not observed at 1 μM which is an extremely low concentration for induction of dye aggregation. This observation further suggests that the new emitting species is a molecular aggregate formed as a result of higher concentration and irradiation. Irradiation-induced J-aggregation has been reported for other cyanine dyes with different templates.[38] J aggregates are usually characterized by red-shifted absorption and intense fluorescence as compared to the corresponding monomeric species.[37]

In order to further verify irradiation induced J-aggregation formation, fluorescence lifetime measurements were performed. These measurements for [PEG786][NTf_2] nano- and meso-scale GUMBOS in water revealed an extremely short component of 69 ps after irradiation. This was the only emitting species as compared to before irradiation which was composed of a longer component of 349 ps. However, as noted, at the lower non-aggregation concentration of 1μM, the appearance of a shorter component was not observed in the fluorescence lifetime measurements after irradiation. Similar results were obtained for

[PEG786][AOT] nano- and meso-scale GUMBOS at higher concentrations. These results are summarized in Table 1. J-aggregation is often characterized by short lifetimes and enhanced fluorescence. Thus, the combination of steady state fluorescence, kinetic studies, and fluorescence lifetime confirms irradiation induced J-aggregation and enhanced fluorescence of the PEGylated nano- and meso-scale GUMBOS.

3.c. Studies of Resistance to Nonspecific Protein Adsorption

Absorption difference spectroscopy is often used to study the interaction between dyes and proteins.[36] The absorption spectrum of the unmodified dye [IR786][I] in water has a broad maximum at 764 nm (Figure S5 of Supporting information). In contrast, the spectrum of [IR786][I] in the presence of BSA is characterized by a maximum at 785 nm with a narrow peak. Thus, a considerable difference in absorbance was observed due to formation of an IR786 BSA complex. For determination of the dye BSA binding process, 20 μM of unmodified [IR786][I] was titrated with increasing amounts of BSA, and 0.5 mg/mL of BSA was titrated with increasing amounts of [IR786][I]. The intensity of the 785 nm peak in each spectrum was plotted against the BSA concentration (Figure 6 A), or dye concentration (Figure 6 B). In both studies, the plots appeared to be linear. These results suggest that the [IR786][I] has a strong interaction with BSA, and the dye-BSA complex concentration is directly proportional to both the dye and BSA concentration.

Similar studies to those described in the previous paragraph were conducted between PEGylated dye, [PEG786][I], and BSA. A difference in absorbance was observed in [PEG786][I] and BSA mixture compared to [PEG786][I] in PBS solution (Supporting information Figure S6). A peak shift from 625 nm to 645 was ascribed to the presence of PEG786 – BSA complex. Evaluation of the titration studies showed that the titration curve was saturated at a concentration of 0.3 mg/mL BSA with a constant dye concentration (Figure 7 C). When the BSA concentration was held constant at 0.5 mg/mL, increasing the dye concentrations showed negligible effect on the intensity of the 645 nm peak for difference spectra (Figure 7D). Therefore, [PEG786][I] interacts very weakly with BSA and binding to BSA follows a saturation curve.

3.d. In vitro Cytotoxicity Assay of PEG786 GUMBOS

Cellular toxicity of fluorescent NIR nano-particles is a prime limitation which restricts application to living cell imaging.[39] Quantum dots are photostable fluorescent NIR nano-particles with high luminescent efficiency; however, these nano-particles are not always suitable for application in humans due to cytotoxic effects.[40-42] Indocyanine green (ICG), in contrast, has been approved by the FDA for human use because of its low toxicity regardless of its poor photostablity and low quantum yield in aqueous media. However, research has demonstrated increased toxicity with an increase in ICG concentration, which limits the application of ICG at higher concentrations.[43]

Evaluation of our *in vitro* cytotoxicity data suggests that the cytotoxicity of PEG786 GUMBOS is similar to [IR786][I] at low concentrations, but significantly different from [IR786][I] at high concentrations (Figure 8). When the concentration is less than 15 μM, both PEGylated and un-PEGylated dye show low toxicity to cells, and there is no significant

differences between [IR786][I] and PEG786 GUMBOS. Further examination of the results of the modified and unmodified dyes suggests that PEGylation significantly reduces the cytotoxicity of [IR786][I] at high concentrations. For example, the average cell viabilities in wells containing [PEG786][I], [PEG786][NTf_2] and [PEG786][AOT] are 40.7%, 51.3% and 55.7% at a concentration of 30 μM, while the average cell viability in wells containing the same concentration of [IR786][I] is 8.4% which is lower than that of dead control (10.3 %). This indicates that [IR786][I] completely inhibited cell proliferation at this concentration. This phenomenon can be ascribed to the formation of PEG786 nano- and meso-scale GUMBOS comprised of molecular self-assemblies with the hydrophobic dye skeleton facing the core of the assembly and the hydrophilic PEG chain on the surface at high concentrations. Thus, PEG chains appear to protect the dye from direct contact with the cells, thereby decreasing its toxicity. This result suggests that PEG786 GUMBOS are suitable to be employed for cellular imaging at high concentrations.

4. Conclusions

We have successfully synthesized PEG modified IR786 GUMBOS by simple variations of the associated counter anions. After modification, the new dyes showed very different properties as compared to the unmodified dye, which appear to be a result of formation of self-assemblies in water. A large Stokes shift of the PEG786 GUMBOS is attributed to intramolecular charge transfer (ICT) between the pyramidal and planar conformations in the excited states. PEG786 nano- and meso-scale GUMBOS also exhibit a reduced binding constant with BSA and reduced cytotoxicity at higher concentration. This is likely due to protection from PEG chains located on the surface of the nano- and meso-scale GUMBOS.

In addition to the above properties, photostability of PEG786 nano- and meso-scale GUMBOS varies with changes in anion. AOT and NTf_2 are shown to improve the photostablity of PEG786 nano- and meso-scale GUMBOS. We have also demonstrated that improved photostablity of [PEG786][NTf_2] nano- and mesoscale GUMBOS is a result of irradiation induced changes in dye molecule stacking, which lead to J-aggregation. Most importantly, the observation that PEGylation of IR786 followed by anion exchange with suitable anions leads to enhanced fluorescence upon irradiation and reduced cytotoxicity at higher concentrations may provide many potential applications for biomedical imaging using NIR fluorescence.

Supplementary Material

Refer to Web version on PubMed Central for supplementary material.

Acknowledgments

Isiah M. Warner acknowledges financial support from the National Science Foundation (NSF) (grant no.CHE-0616827) and National Institute of Health (NIH) (grant no. 1R01GM079670).

Reference

1. Erogbogbo F, Yong KT, Roy I, Hu R, Law WC, Zhao WW, Ding H, Wu F, Kumar R, Swihart MT, Prasad PN. In Vivo Targeted Cancer Imaging, Sentinel Lymph Node Mapping and Multi-Channel

Imaging with Biocompatible Silicon Nanocrystals. Acs Nano. 2010; 5(1):413–423. [PubMed: 21138323]

2. Foy SP, Manthe RL, Foy ST, Dimitrijevic S, Krishnamurthy N, Labhasetwar V. Optical Imaging and Magnetic Field Targeting of Magnetic Nanoparticles in Tumors. Acs Nano. 2010; 4(9):5217–5224. [PubMed: 20731413]
3. Bringley JF, Penner TL, Wang RZ, Harder JF, Harrison WJ, Buonemani L. Silica nanoparticles encapsulating near-infrared emissive cyanine dyes. Journal of Colloid and Interface Science. 2008; 320(1):132–139. [PubMed: 18191871]
4. Morgan TT, Muddana HS, Altinoglu EI, Rouse SM, Tabakovic A, Tabouillot T, Russin TJ, Shanmugavelandy SS, Butler PJ, Eklund PC, Yun JK, Kester M, Adair JH. Encapsulation of Organic Molecules in Calcium Phosphate Nanocomposite Particles for Intracellular Imaging and Drug Delivery. Nano Letters. 2008; 8(12):4108–4115. [PubMed: 19367837]
5. Liong M, Lu J, Kovochich M, Xia T, Ruehm SG, Nel AE, Tamanoi F, Zink JI. Multifunctional inorganic nanoparticles for imaging, targeting, and drug delivery. Acs Nano. 2008; 2(5):889–896. [PubMed: 19206485]
6. Ow H, Larson DR, Srivastava M, Baird BA, Webb WW, Wiesner U. Bright and stable core-shell fluorescent silica nanoparticles. Nano Letters. 2005; 5(1):113–117. [PubMed: 15792423]
7. Fuller JE, Zugates GT, Ferreira LS, Ow HS, Nguyen NN, Wiesner UB, Langer RS. Intracellular delivery of core-shell fluorescent silica nanoparticles. Biomaterials. 2008; 29(10):1526–1532. [PubMed: 18096220]
8. Weissleder R. A clearer vision for in vivo imaging. Nature Biotechnology. 2001; 19(4):316–317.
9. Altinoglu EI, Russin TJ, Kaiser JM, Barth BM, Eklund PC, Kester M, Adair JH. Near-Infrared Emitting Fluorophore-Doped Calcium Phosphate Nanoparticles for In Vivo Imaging of Human Breast Cancer. Acs Nano. 2008; 2(10):2075–2084. [PubMed: 19206454]
10. Michalet X, Pinaud FF, Bentolila LA, Tsay JM, Doose S, Li JJ, Sundaresan G, Wu AM, Gambhir SS, Weiss S. Quantum dots for live cells, in vivo imaging, and diagnostics. Science. 2005; 307(5709):538–544. [PubMed: 15681376]
11. Liu W, Howarth M, Greytak AB, Zheng Y, Nocera DG, Ting AY, Bawendi MG. Compact biocompatible quantum dots functionalized for cellular imaging. Journal of the American Chemical Society. 2008; 130(4):1274–1284. [PubMed: 18177042]
12. Venisnik KM, Olafsen T, Loening AM, Iyer M, Gambhir SS, Wu AM. Bifunctional antibody-Renilla luciferase fusion protein for in vivo optical detection of tumors. Protein Engineering Design & Selection. 2006; 19(10):453–460.
13. Maxwell D, Chang Q, Zhang X, Barnett EM, Piwnica-Worms D. An Improved Cell-Penetrating, Caspase-Activatable, Near-Infrared Fluorescent Peptide for Apoptosis Imaging. Bioconjugate Chemistry. 2009; 20(4):702–709. [PubMed: 19331388]
14. Murphy CJ, Gole AM, Hunyadi SE, Stone JW, Sisco PN, Alkilany A, Kinard BE, Hankins P. Chemical sensing and imaging with metallic nanorods. Chemical Communications. 2008; (5):544–557. [PubMed: 18209787]
15. Weissleder R, Tung CH, Mahmood U, Bogdanov A. In vivo imaging of tumors with protease-activated near-infrared fluorescent probes. Nature Biotechnology. 1999; 17(4):375–378.
16. Cheng Z, Levi J, Xiong ZM, Gheysens O, Keren S, Chen XY, Gambhir SS. Near-infrared fluorescent deoxyglucose analogue for tumor optical imaging in cell culture and living mice. Bioconjugate Chemistry. 2006; 17(3):662–669. [PubMed: 16704203]
17. Becker A, Hessenius C, Licha K, Ebert B, Sukowski U, Semmler W, Wiedenmann B, Grotzinger C. Receptor-targeted optical imaging of tumors with near-infrared fluorescent ligands. Nature Biotechnology. 2001; 19(4):327–331.
18. Klohs J, Wunder A, Licha K. Near-infrared fluorescent probes for imaging vascular pathophysiology. Basic Research in Cardiology. 2008; 103(2):144–151. [PubMed: 18324370]
19. Luo S, Zhang E, Su Y, Cheng T, Shi C. A review of NIR dyes in cancer targeting and imaging. Biomaterials. 2011; 32(29):7127–38. [PubMed: 21724249]
20. Bwambok DK, El-Zahab B, Challa SK, Li M, Chandler L, Baker GA, Warner IM. Near-Infrared Fluorescent NanoGUMBOS for Biomedical Imaging. Acs Nano. 2009; 3(12):3854–3860. [PubMed: 19928781]

21. Das S, Bwambok D, Ei-Zahab B, Monk J, de Rooy SL, Challa S, Li M, Hung FR, Baker GA, Warner IM. Nontemplated Approach to Tuning the Spectral Properties of Cyanine-Based Fluorescent NanoGUMBOS. Langmuir. 2010; 26(15):12867–12876. [PubMed: 20583774]
22. Patonay G, Salon J, Sowell J, Strekowski L. Noncovalent labeling of biomolecules with red and near-infrared dyes. Molecules. 2004; 9(3):40–49. [PubMed: 18007410]
23. Masotti A, Vicennati P, Boschi F, Calderan L, Sbarbati A, Ortaggi G. A novel near-infrared indocyanine dye - Polyethylenimine conjugate allows DNA delivery imaging in vivo. Bioconjugate Chemistry. 2008; 19(5):983–987. [PubMed: 18429627]
24. Lee YEK, Smith R, Kopelman R. Nanoparticle PEBBLE Sensors in Live Cells and In Vivo. Annual Review of Analytical Chemistry. 2009; 2:57–76.
25. Zhang ZR, Achilefu S. Synthesis and evaluation of polyhydroxylated near infrared carbocyanine molecular probes. Organic Letters. 2004; 6(12):2067–2070. [PubMed: 15176820]
26. Lee H, Mason JC, Achilefu S. Heptamethine cyanine dyes with a robust C C bond at the central position of the chromophore. Journal of Organic Chemistry. 2006; 71(20):7862–7865. [PubMed: 16995699]
27. Peng XJ, Song FL, Lu E, Wang YN, Zhou W, Fan JL, Gao YL. Heptamethine cyanine dyes with a large stokes shift and strong fluorescence: A paradigm for excited-state intramolecular charge transfer. Journal of the American Chemical Society. 2005; 127(12):4170–4171. [PubMed: 15783189]
28. Lu W, Wan J, Zhang Q, She ZJ, Jiang XG. Aclarubicin-loaded cationic albumin-conjugated pegylated nanoparticle for glioma chemotherapy in rats. International Journal of Cancer. 2007; 120(2):420–431.
29. Levy DE, Ding ZL, Hu CW, Zalipsky S. PEGylated iminodiacetic acid zinc complex stabilizes cationic RNA-bearing nanoparticles. Bioorganic & Medicinal Chemistry Letters. 20(18):5499–5501. [PubMed: 20696578]
30. Lipka J, Semmler-Behnke M, Sperling RA, Wenk A, Takenaka S, Schleh C, Kissel T, Parak WJ, Kreyline WG. Biodistribution of PEG-modified gold nanoparticles following intratracheal instillation and intravenous injection. Biomaterials. 31(25):6574–6581. [PubMed: 20542560]
31. Liu JQ, Setijadi E, Liu YK, Whittaker MR, Boyer C, Davis TP. PEGylated Gold Nanoparticles Functionalized with beta-Cyclodextrin Inclusion Complexes: Towards Metal Nanoparticle-Polymer-Carbohydrate Cluster Biohybrid Materials. Australian Journal of Chemistry. 63(8):1245–1250.
32. Bazile D, Prud'homme C, Bassoullet MT, Marlard M, Spenlehauer G, Veillard M. Stealth Me.PEG-PLA nanoparticles avoid uptake by the mononuclear phagocytes system. J Pharm Sci. 1995; 84(4):493–8. [PubMed: 7629743]
33. Takahashi T, Yamada Y, Kataoka K, Nagasaki Y. Preparation of a novel PEG-clay hybrid as a DDS material: Dispersion stability and sustained release profiles. Journal of Controlled Release. 2005; 107(3):408–416. [PubMed: 16171884]
34. Chen H, Hu XY, Zhang YX, Li D, Wu ZK, Zhang T. Effect of chain density and conformation on protein adsorption at PEG-grafted polyurethane surfaces. Colloids and Surfaces B-Biointerfaces. 2008; 61(2):237–243.
35. Lu W, Tan YZ, Hu KL, Jiang XG. Cationic albumin conjugated pegylated nanoparticle with its transcytosis ability and little toxicity against blood-brain barrier. International Journal of Pharmaceutics. 2005; 295(1-2):247–260. [PubMed: 15848009]
36. Sereikaite J, Bumeliene Z, Bumelis VA. Bovine serum albumin-dye binding. Acta Chromatographica. 2005; 15:298–307.
37. Mishra A, Behera RK, Behera PK, Mishra BK, Behera GB. Cyanines during the 1990s: A review. Chemical Reviews. 2000100(6):1973–2011.
38. Tachibana H, Sato F, Terrettaz S, Azumi R, Nakamura T, Sakai H, Abe M, Matsumoto M. Light-induced J-aggregation in mixed Langmuir-Blodgett films of selenium-containing cyanine and azobenzene. Thin Solid Films. 1998; 327:813–815.
39. He XX, Wang KM, Cheng Z. In vivo near-infrared fluorescence imaging of cancer with nanoparticle-based probes. Wiley Interdisciplinary Reviews-Nanomedicine and Nanobiotechnology. 2010; 2(4):349–366. [PubMed: 20564463]

40. Hardman R. A toxicologic review of quantum dots: Toxicity depends on physicochemical and environmental factors. Environmental Health Perspectives. 2006; 114(2):165–172. [PubMed: 16451849]

41. Lin P, Chen JW, Chang LW, Wu JP, Redding L, Chang H, Yeh TK, Yang CS, Tsai MH, Wang HJ, Kuo YC, Yang RSH. Computational and ultrastructural toxicology of a nanoparticle, Quantum Dot 705, in mice. Environmental Science & Technology. 2008; 42(16):6264–6270. [PubMed: 18767697]

42. Geys J, Nemmar A, Verbeken E, Smolders E, Ratoi M, Hoylaerts MF, Nemery B, Hoet PHM. Acute Toxicity and Prothrombotic Effects of Quantum Dots: Impact of Surface Charge. Environmental Health Perspectives. 2008; 116(12):1607–1613. [PubMed: 19079709]

43. Ho JD, Tsai RJF, Chen SN, Chen HC. Cytotoxicity of indocyanine green on retinal pigment epithelium Implications for macular hole surgery. Archives of Ophthalmology. 2003; 121(10): 1423–1429. [PubMed: 14557178]

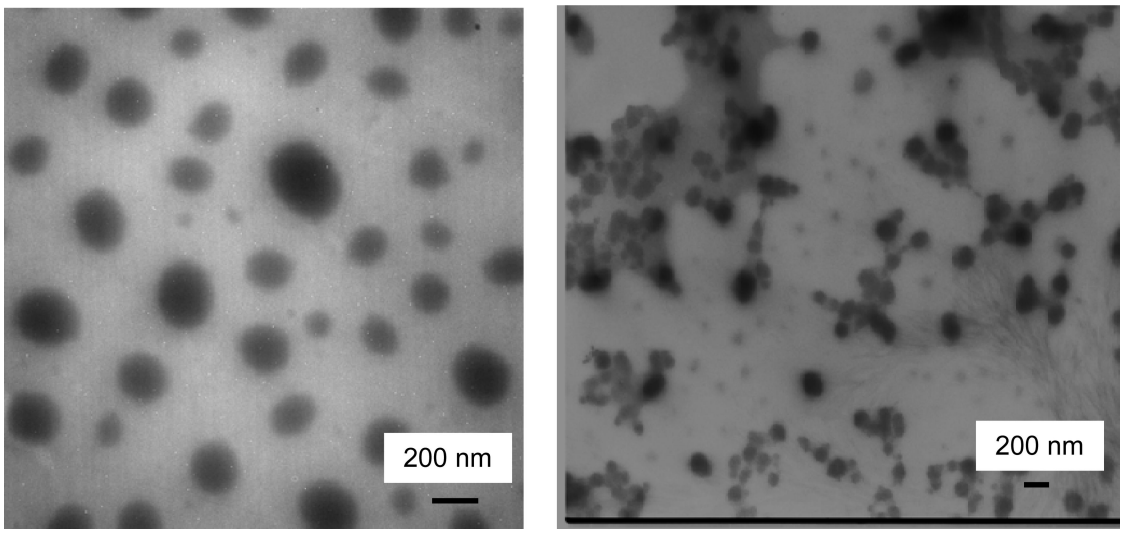

Figure 1.

Transmission electron micrograms of [PEG786][NTf_2] (left) and [PEG786][I] (right) nano- and meso-scale GUMBOS

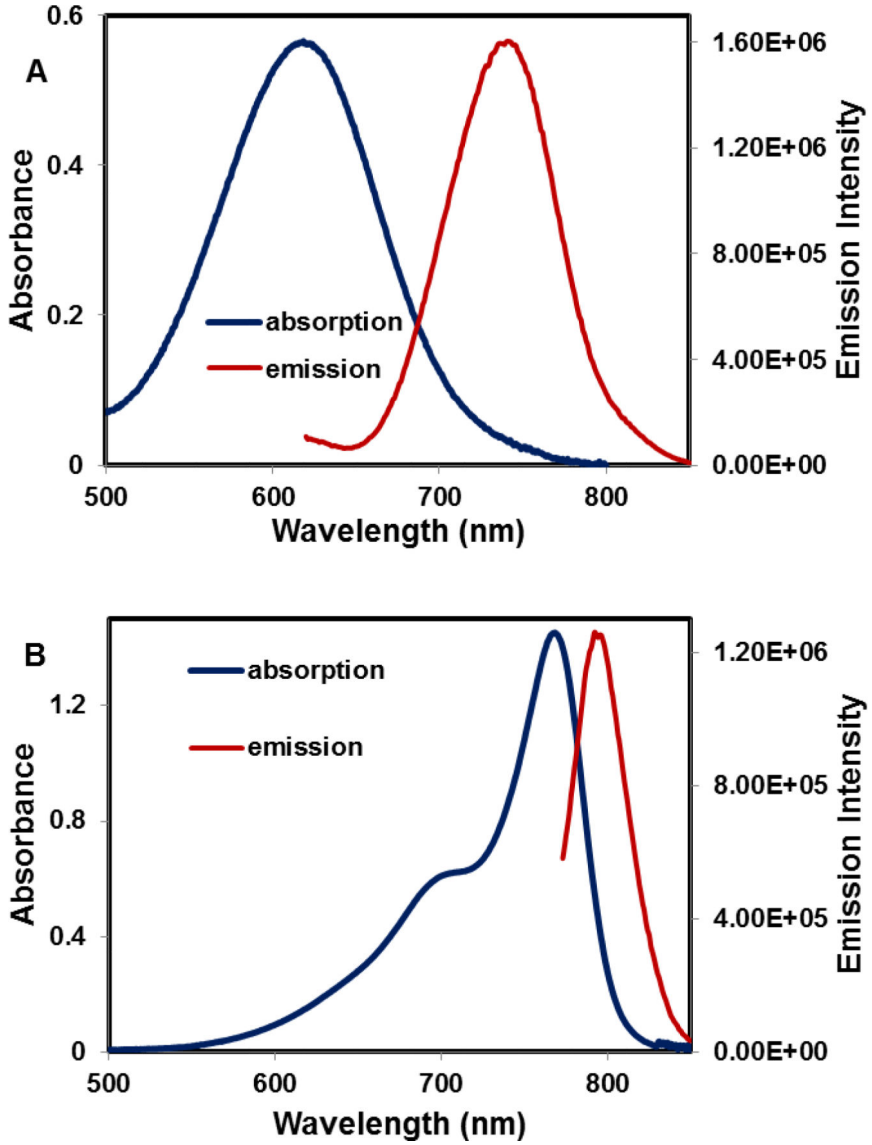

Figure 2.

Absorption (blue) and emission (red) spectra of [PEG786][I] (left) and [IR786][I] (right) in water

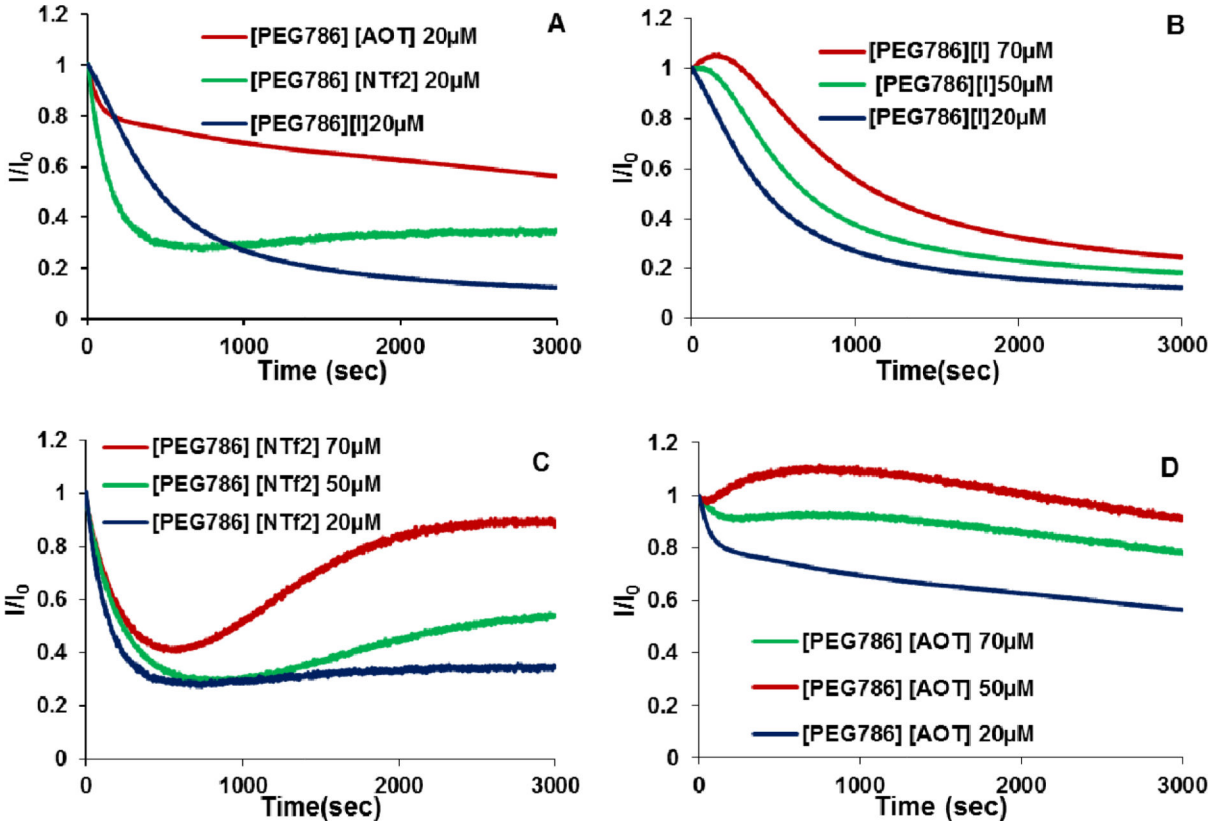

Figure 3.

Effects of anions (A) and concentration (B, C, D) on photostability of PEG786 nano- and meso-scale GUMBOS

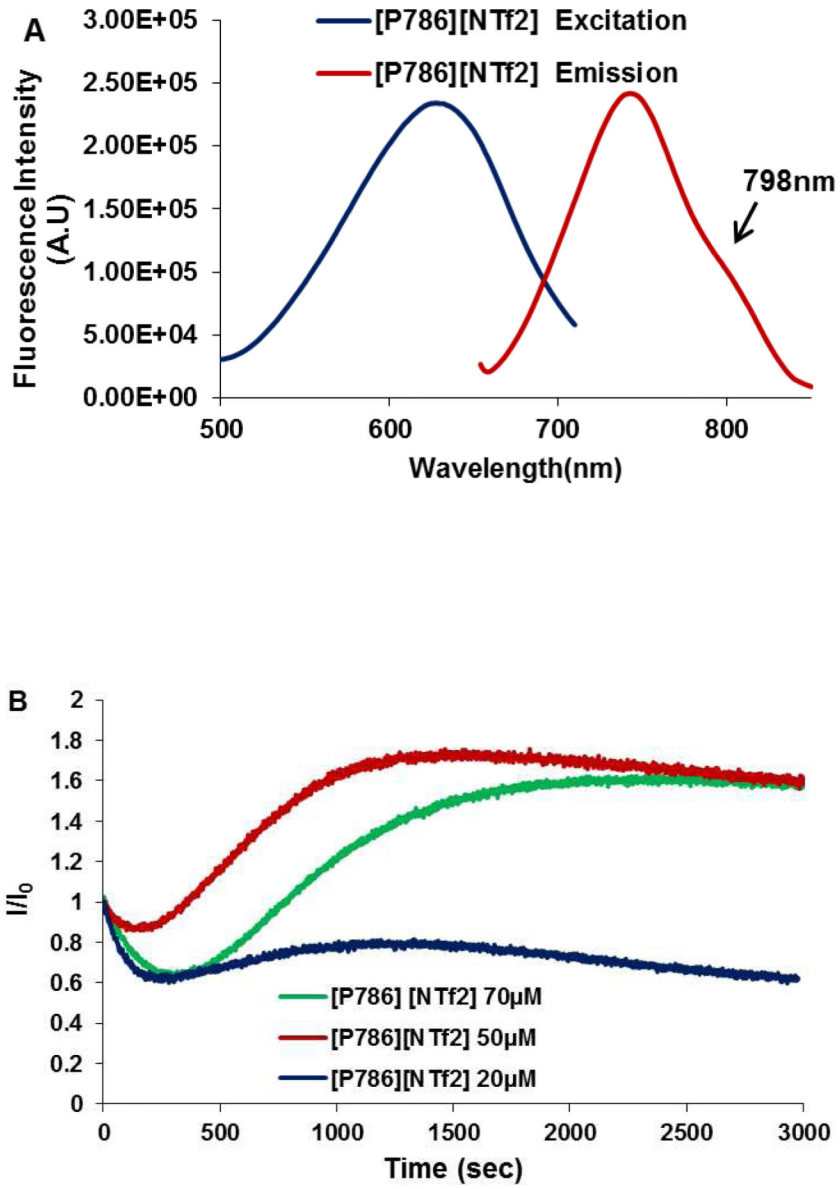

Figure 4.
Photostability study of [PEG786][NTf_2] with emission wavelength at 798 nm

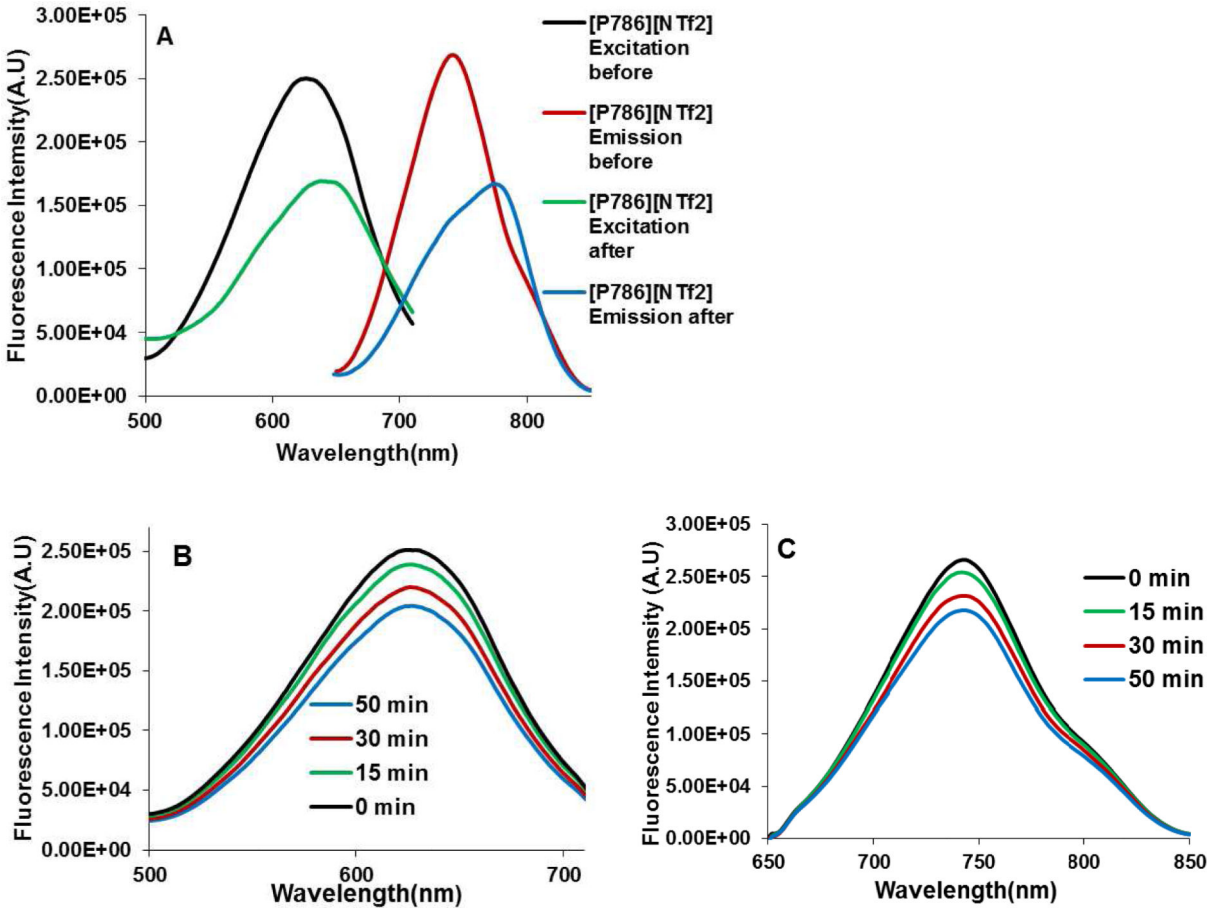

Figure 5.

(A) Excitation (left) and emission (right) spectra of [PEG786][NTf2] (50uM) before and after irradiation. Excitation (B) and emission (C) spectra of [PEG786][NTf2] (50uM) without irradiation

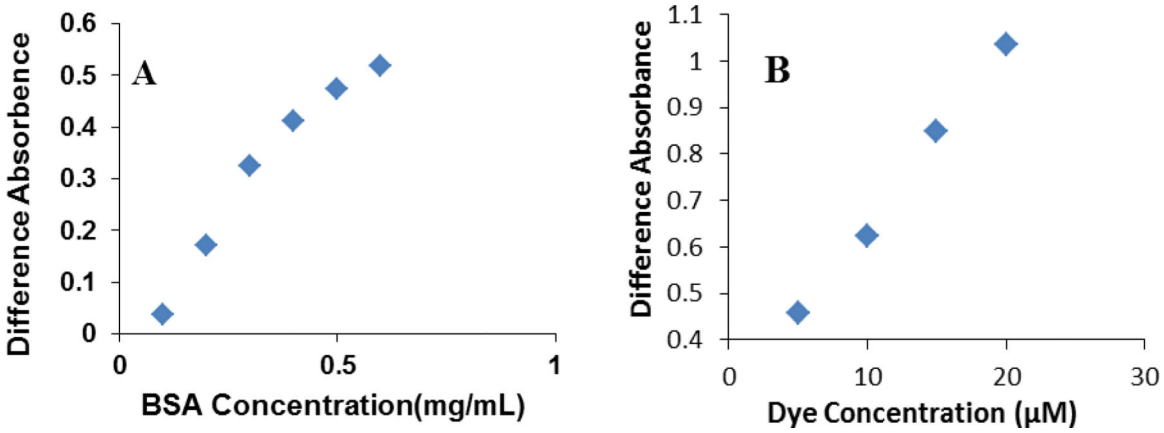

Figure 6.

Titration of BSA with IR786 at λ=785 nm in PBS, pH=7.0. The dye concentration in the sample cuvettes was 20μM (A); the BSA dye concentration in the sample cuvettes was 0.5 mg/mL(B).

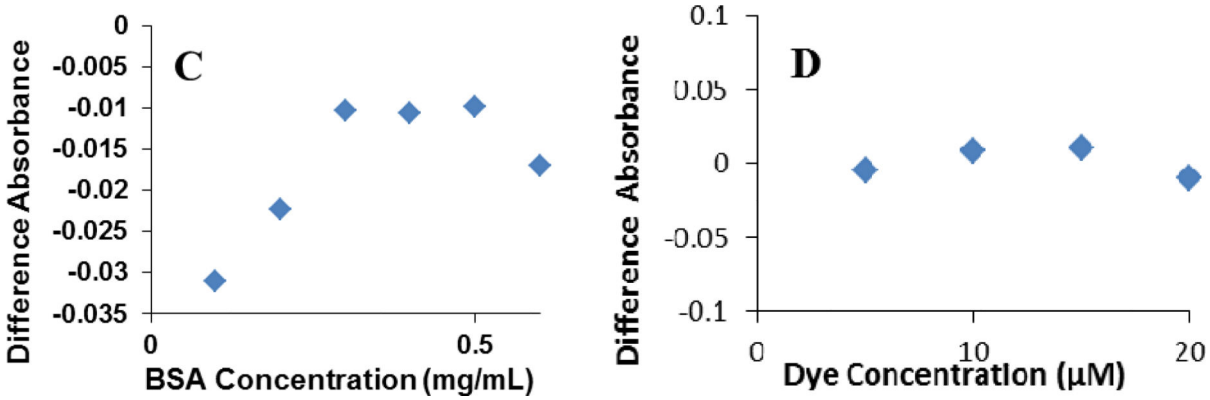

Figure 7.

Titration of BSA with [PEG786][I] at λ=645nm in PBS, pH=7.0. The dye concentration in the sample cuvettes was 20μM (C); the BSA dye concentration in the sample cuvettes was 0.5 mg/mL (D)

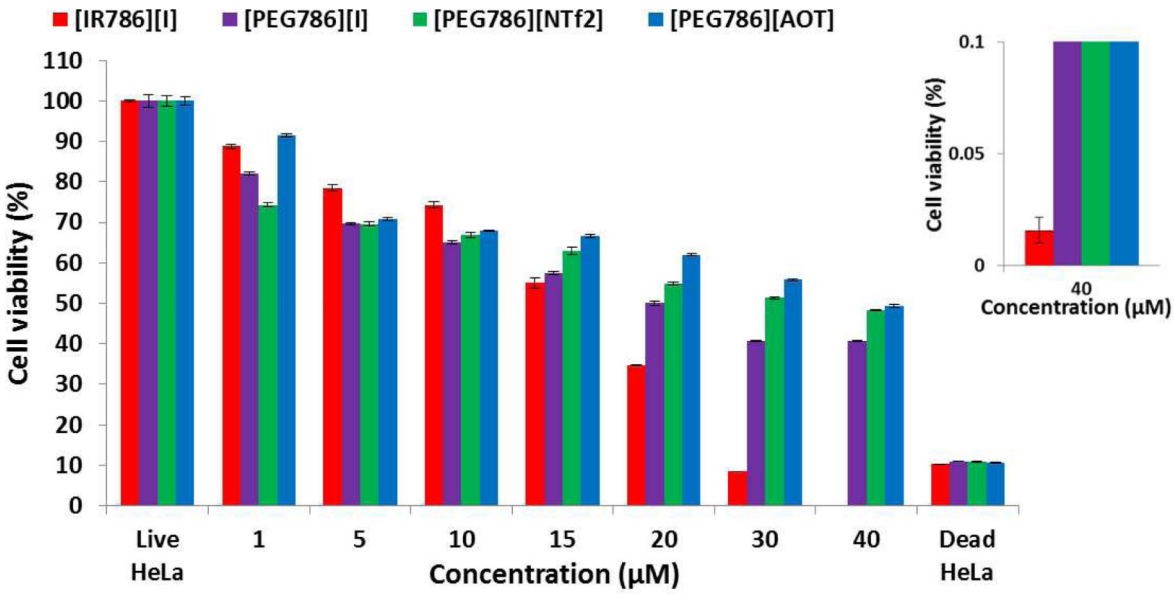

Figure 8.

In vitro cytotoxicity of PEG786 GUMBOS and [IR786][I] on Hela cells as measured by the MTT assay (inset is the cell viability of [IR786][I] at 40 μM). Cell viability is expressed as mean ± S.D. (n = 3).

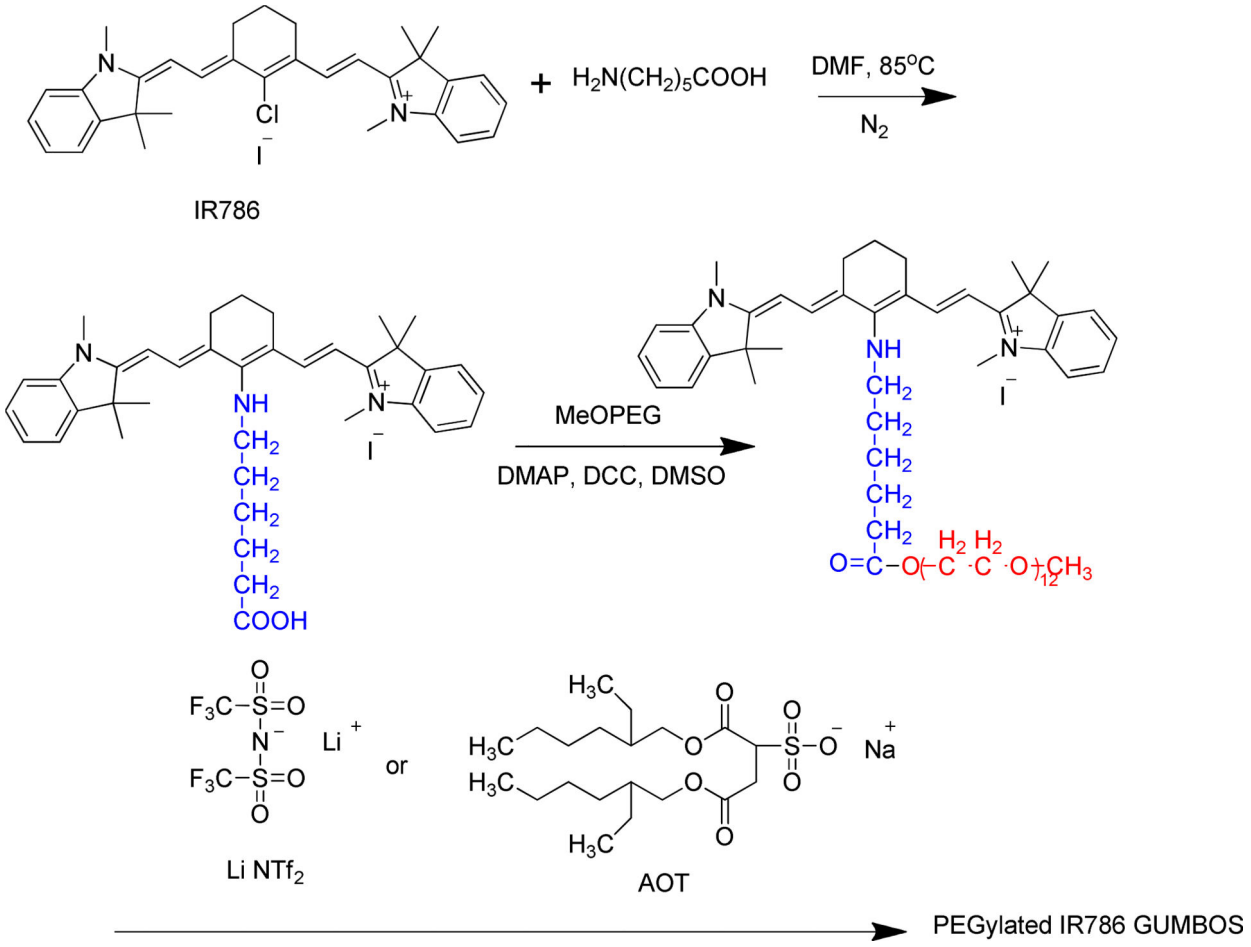

Scheme 1.
Synthesis of PEG786 GUMBOS

Table 1

Lifetime of [PEG786][AOT] and [PEG786][NTf_2] before and after irradiation

System	τ1	al	τ2	a2	χ
1μM [PEG786][AOT] before irradiation	243 ps	l			1.4
1μM [PEG786][AOT] after irradiation	172 ps	l			1.3
50μM [PEG786][AOT] before irradiation	23.5 ps	0.7	325 ps	0.3	1.5
50μM [PEG786][AOT] after irradiation	32.3 ps	0.9	190 ps	0.1	1.5
1μM [PEG786][NTf_2] before irradiation	146 ps	l			1.4
1μM [PEG786][NTf_2] after irradiation	272 ps	l			1.2
50μM [PEG786][NTf_2] before irradiation	349 ps	l			1.2
50μM [PEG786][NTf_2] after irradiation	69 ps	0.99	395 ps	0.01	1.8